

## Pamukkale Üniversitesi Mühendislik Bilimleri Dergisi

## Pamukkale University Journal of Engineering Sciences



## Behavior of geogrid-reinforced concrete slabs subjected to contact explosions

# Geogrid takviyeli beton döşemelerin temas patlamasına karşı davranışının araştırılması

Dursun Bakır1\*, Sedat Savas2

<sup>1</sup>Bitlis Eren University, Bitlis, Türkiye. dursunbakir23@gmail.com

<sup>2</sup>Fırat University, Elazığ, Türkiye. ssavas@firat.edu.tr

Received/Geliş Tarihi: 29.06.2025 Accepted/Kabul Tarihi: 08.09.2025 Revision/Düzeltme Tarihi: 04.09.2025

doi: 10.5505/pajes.2025.40204 Research Article/Araştırma Makalesi

#### **Abstract**

Bomb attacks are occurring in the world due to the increasing hot and cold wars. In this study, the contact explosion, which affects the resistance of the structure the most, was investigated among these attacks. Since the explosive is in contact with the surface of the structure in contact explosion, the reaction of the structure in bending and shear behavior due to sudden dynamic loading differs from other loads. In our experimental study, 50x50x15 cm reinforced concrete slabs reinforced with steel wire mesh, wire fence and geogrid building materials were produced in order to compare the behavior of concrete against explosion. In contact with these plates, 577 gr explosive was applied and detonated. In the experiments, the contact explosion reactions of geogrid reinforced concrete and steel-reinforced concrete and unreinforced concrete were compared. As a result of the experiments, it was determined that the concrete reinforced with wire fence and geogrid is applicable against contact explosion.

**Keywords:** Contact explosion, Geogrid, Steel wire mesh, Steel wire fence.

#### ö

Dünyada gittikçe artan sıcak ve soğuk savaşlardan kaynaklı bombalı saldırılar meydana gelmektedir. Çalışmamızda bu saldırılar içerisinde yapının direncini en fazla etkileyen temas patlaması araştırılmıştır. Temas patlamasında patlayıcı yapı yüzeyi ile temas halinde olduğu için ani dinamik yüklemeden dolayı yapı eğilme ve kesme davranışında reaksiyonlarda diğer yüklemlere göre göstermektedir Patlama olayında bir mühendislik yapısının göstereceği hasarı azaltmak için hem dayanıklılık hem de ekonomik performansı göz önüne almak gereklidir. Yaptığımız deneysel çalışmada betonun patlama karşısındaki davranışlarını kıyaslamayabilmek için hasır çelik, telçit ve geogrid yapı malzemeleri ile güçlendirilmiş 50x50x15 cm BA plaklar üretilmiştir. Bu plaklara temas halinde 577 g patlayıcı uygulanarak patlatılmıştır. Deneylerde geogrid takviyeli beton ile çelik donatılı beton ve donatısız betonun temas patlaması reaksiyonları ile karşılaştırılmıştır. Yapılan deneyler sonucunda telçit ve geogrid ile güçlendirilmiş betonun temas patlamasına karşı uygulanabilir olduğu belirlenmiştir.

Anahtar kelimeler: Temas patlaması, Geogrid, Hasır çelik, Telçit.

#### 1 Introduction

When we look at the bomb attacks in general, they are experienced in the form of contact, close contact and distant explosions. In these explosions, cracks, fragmentation and separations occur according to the damage levels [1]. When the tensile strength due to the ambient pressure caused by the explosion on the concrete surface in contact is greater than the tensile strength of the concrete, the cracks increase significantly. In addition, when the impulse effect on the surface is more than the maximum bearing load of the structure, separations occur [2]. Since the explosive is left in contact with the concrete surface and detonated in the contact explosion, the concrete must meet the tensile stresses that occur during the explosion [3],[4]. In recent years, many studies have been carried out on contact explosion, reinforced with building material or modified reinforcement plan and structure. For example, increasing the explosion resistance of the reinforced concrete slab by changing the reinforcement plan and spacing [5],[6], strengthening it by using construction materials such as steel fiber in certain proportions [7], increasing the explosion

protection of concrete with steel fiber additives[8], hybrid fiber reinforced concrete (HFRC) to increase the explosion resistance of panels and compare it with polypropylene (PP), polyvinyl alcohol (PVA) and steel fiber reinforcements [9]. Production of coatings knitted with pure polyurea and glass fiber to prevent cracking and separation of concrete in explosion [10], increasing the resistance against explosion by providing high tensile strength by using polyisocyanateoxazodone (POZD) with high polymer properties [11], shear strength using steel, concrete-steel composite and increasing the tensile strength of the concrete by increasing the ductility and increasing the resistance to the explosion load [12]. Producing crack-resistant and high-durability concrete using ultra-high performance cement-based composite (UHPCC) and providing resistance against impact and explosion [13],[14] are studies that affect the performance of concrete.

Another material used in highway and railway structures, geogrid is used to stabilize weak soils to improve the stiffness of foundations and to meet tensile stress [15]-[17]. Especially in weak soils, settlements on the ground have decreased with geogrid coating and the carrying capacity has increased

<sup>\*</sup>Corresponding author/Yazışılan Yazar

considerably [18],[19]. First, Becham and mills used it in asphalt layers in their study. They observed that cracking, splitting and fragmentation behaviors on the road decreased It is important to examine the behavior of this material in concrete[20]. When the behavior of geogrid in concrete against compression and bending is examined, it is seen that it performs better than conventional concrete and steel fiber concrete under applied axial pressure [21]. Rajesh Kumar et al. In their study, flexural (bending) was applied to steel reinforced concrete and geogrid reinforced concrete samples, and the load bearing capacity, deflection and energy absorption of geogrid reinforced concrete increased by 25%, 6.5% and 23%, respectively[22]. When impact tests were made on geogrid added concrete, it was observed that the impact resistance was better than conventional concrete, and the cracks were more pronounced[23]. Xiaoyu Meng et al. In their study, they found that in the four-point bending tests applied to concrete beams prepared with different aggregate sizes, geogrid positions and geogrid layer numbers, they had positive effects on the permeability of the concrete compared to unreinforced concrete, and increased the bending strength by 52% [24]. TJ Vijay et al. In their study, six reinforced concrete slab samples prepared with steel and geogrid reinforcement layers were prepared. A cylindrical hammer with a hemispherical impact tip with a radius of 80 mm applied a weight drop impact test from a distance of 1.2 meters. Damage modes, energy, ductility index and maximum deflection of each impact were investigated. The geogrid acted resistant to crushing of the concrete by spreading the impact stress over a wider area. It also reduced the formation and propagation of cracks by slowing down [25]. Geogrid provided ductility in asphalt layers and minimized crater dimensions in impact loadings. Reinforced concrete layer and Engineered Cementitious Composites layer respectively under the geogrid reinforced asphalt layer. The crater dimensions were compared by detonating 7.3 kg TNT at a distance of 17cm, equivalent to the layered reference sample reinforced with normal strength concrete and the layers reinforced with Geogrid. The geogrid layer reduced the crater dimensions by approximately 60%, and the integrity of the structure was preserved without fragmentation [26]-[27].

When the studies examining the structural elements using steel wire mesh (SWM), a ductile material, are examined, it is understood that it distributes the stress uniformly and increases the ductility and fracture stresses when compared to conventional reinforced concrete [28]-[32]. In this study, in which impact load was applied with this reinforcement, a central square or rectangular load was applied to a contact area of  $80 \times 80$  mm or  $55 \times 360$  mm, respectively, on the samples of 36x49 cm dimensions, which were simply supported on four sides on a steel frame. The samples were prepared for comparison with both conventional concrete and reinforced with SWM (Figure 1). Specimen deflection with rectangularloaded SWM was significantly increased by approximately 60% and 288%, respectively, compared to those tested under square patch load. Compared to conventionally reinforced plates, drilling behavior did not change[33].

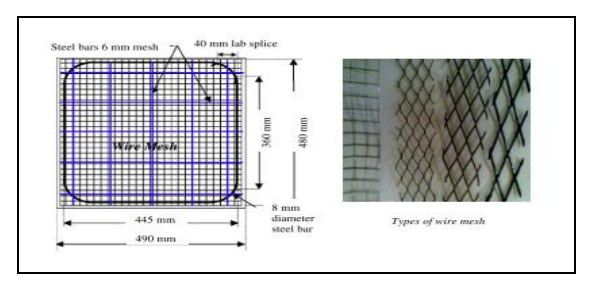


Figure 1. SWM reinforcement details of the slabs [33].

Jun Liv et.al. 2016), they stated that current design and research practices mainly focus on structural responses and damage under explosions in the far field or near, and explosion scenarios involving contact explosions have not been extensively investigated. Under contact explosions, a high degree of local damage caused by severe stress wave propagation is observed and this mode of damage is significantly different from other types of dynamic loading to which structural members usually respond in bending or shear mode. In their studies, performance measurements were made of normal strength concrete and reinforced concrete slabs with steel wire mesh (wire mesh with 1mm diameter and 6mm spacing) [34]. 1kg of TNT is contacted in the middle of this plate, which is reinforced with SWM and has a concrete compressive strength of 40N/mm<sup>2</sup>. A crater of 40 and 42 cm in size was formed on the surface (Figure 2).

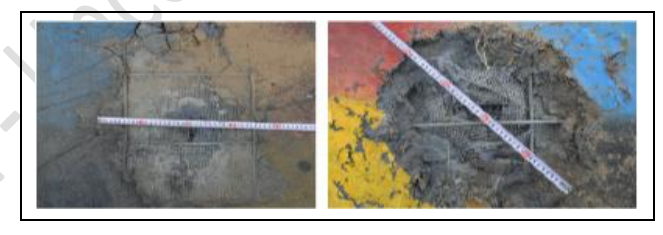


Figure 2. Post-explosion damage level of SWM reinforced plate [34].

Jun li et al. In their study conducted in 2017, steel wire mesh with a mesh size of  $6.35 \times 6.35$  mm and a wire diameter of 1 mm was used. The prepared slabs of 2000 mm length, 800 mm width and 120 mm thickness, with a concrete compressive strength of 60N/mm<sup>2</sup>, were field tested under 1 kg of TNT contact explosion. It has been shown that 20cm to 40cm steel wire mesh reinforced slab develops local membrane effect and better explosion proof ability when subjected to blast loads compared to slabs without steel wire mesh. In the steel wire mesh placed in 10, 20 and 30 layers, the crater widths were measured as 26 cm, 22 cm and 19 cm, respectively, after the explosion, and the plates were drilled [35]. In this research, contact explosion was applied to prepared plates of 50x50x15 cm dimensions, reinforced with wire mesh and geogrid, without reinforcement. Permanent deformations in the plates under the blast load were observed and comparisons were made with the crater diameter and depth. Geogrid and wire mesh reinforcements did not directly modify the crater geometry; nevertheless, by changing the nature of the damage, they restricted fracture propagation, enhanced energy absorption capacity, and aided in maintaining structural integrity.

## 2 Experimental study

In order to compare the behavior of non-reinforced concrete and concrete slabs reinforced with 4 different building materials against contact explosive load, 30 pieces of 50x50x15 cm slabs with a cylindrical compressive strength of  $30N/mm^2$  were produced for each sample. In the experimental study, non-reinforced and reinforced concrete slabs were fabricated to compare the explosive resistance of different materials. The samples have the same concrete strength and mix (Table1). The samples were prepared for testing following a 28-day curing period.

Table 1. Concrete mixing ratios.

Cement	16%
Aggregate size (7-14 mm)	35.40%
Aggregate size (3-9 mm)	4.40%
Sand	37.60%
Water	6.40%
Additive	0.20%

#### 2.1 Steel wire mesh

The Q131/131 [36] (Table2) was placed in 50x50x15cm molds, two rows down and two rows up, staggered (Figure 3). After the SWM was placed, the prepared concrete mixture was placed on the vibration table and exposed to vibration. Then, water curing was applied to the concrete samples removed from the molds for 28 days.

Table 2. Q131/131 steel wire mesh.

Reinforcement range	150 m
Reinforcement diameter	5.0 mm
Reinforcement cross-sectional area	$1.31 \text{ m}^2$
Bidirectional reinforcement rate	0.35%

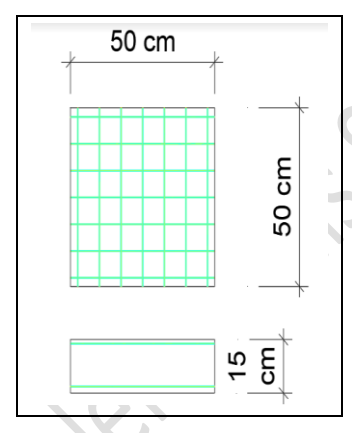


Figure 3. Formwork sizes of wire mesh steel.

## 2.2 Geogrid

As seen in Figure 4, the geogrids were prepared in 6, 9 and 12 layers by placing 1 cm of concrete between them. These layer numbers were determined considering the thinness of the material and the concrete mold. It is arranged according to the maximum number of layers of the geogrid in the mold placement. No interface procedure, including surface roughening or pre-coating, was conducted prior to or during the placement of the geogrid in the concrete. The geogrid was installed concurrently with the fresh concrete pour. The adhesion process fundamentally relies on the mechanical interlocking and compaction afforded by the concrete matrix. The properties of the geogrid material used in this study were determined by performing experiments (Table 3).



Figure 4. Concrete formwork with geogrid and pouring.

Table 3. Geogrid material properties.

Raw				
materials		High Densi	ity Polyeth	ylene
				EN ISO
Intensity	0.94	g/cm <sup>3</sup>	-10%	1183[37]
				ASTM D
Carbon Black	1-3	%	-10%	1603[38]
				EN ISO 9863-
Thickness	>4.00	mm	-10%	1[39]
Unit Surface				EN ISO
Weight	>800	g/m <sup>2</sup>	-10%	9864[40]
Bearing				
capacity	160 kM	N/m		

#### 2.3 Steel wire fence

Galvanized steel wire is a kind of material made by hot dipping into zinc. This material is highly resistant to rust due to zinc. The reason for choosing this type of material is to ensure that steel bars with a small cross-sectional area meet the cutting and punching forces. The material properties of the steel wire fence used are given in Table 4 and tensile tests were carried out in the laboratory.

Table 4. Steel wire fence specifications.

Wire Diameter	2.90 mm
Sieve size	40 mm
Tensile Strength	400-500 N/mm <sup>2</sup>
Elongation	%16-32
Steel Quality	SAE

As can be seen in Figure 5, the material with a mesh size of 4 cm was prepared in 50x50x15 cm molds with 45x45 cm dimensions. It was placed in the prepared formworks in 7, 10 and 13 layers by vibration and left for the setting process (Figure 6).



Figure 5. Preparation of galvanized wire.



Figure 6. Concrete formworks of prepared Galvanized Wire and pouring.

## 3 Determination of TNT equivalence

The explosive used in the experiments is Nitroglycerin based (TNG), Powergel magnum365(Table 5). It is extremely safe against blasting by explosive, friction, impact and other mechanical effects and is highly resistant to water [41].

Table 5. TNG properties [41].

Explosive Properties Used in the Experiment	
Ideal Detonation Velocity (m/s)	6140
Ideal Detonation Pressure (atm)	112900
Ideal Detonation Temperature (K)	3106
Density(gr/cm³)	1.20
Water Resistance	Great
Ideal Explosion Temperature (kJ / Kg.)	4370
Ideal Gas Volume (Lt / Kg)	873
Relative Effective Energy (%)in comparison to ANFO	129
Relative Bulk Strength (%)in comparison to ANFO	193

In order to determine the TNT equivalence according to the current explosive we use, field experiments were carried out(Figure 8). Free field pressure transducer pencil(Figure 7) used in the experiment obtained ambient pressure-time data from test blasts (Figure 11). This pressure pen is mounted in an axial direction to the detonation source and aligned perpendicular to the blast surface. Free field pressure transducer is placed on the ground with a steel bar element to fix the pressure pen on the ground surface (Figure 9).



Figure 7. PCB Piezoelectric series pressure transducer pencil.

The data acquisition (DAQ) system, Free field pressure transducer (ambient pressure pen), Oros-or36 branded data logger device with 16 channels that can receive 51200 data per second from a single channel and a laptop computer with NV gate software [42]. This Free field pressure transducer received data from the data logger with coaxial cables of 20 m length.



Figure 8. The experimental setup.

The distance of the sensor placed in the experimental setup to the explosive is 3.2 m [43]. The distance of the explosive from

the ground (stand-off distance), the height of the steel bars where the sensors are placed (Sensor Elevation) and the explosive-sensor distances are given in Table 6.

Table 6. Layout of the Experimental setup.

Stand-off Distance m	1.855
Explosive Weight (W kg)	0.91
Sensor Elevation(m)	1.85
Explosive-Sensor Distance (m)	3.2



Figure 9. Sensor placement.

$$Z = \frac{R}{W^{\frac{1}{3}}} \tag{1}$$

Explosives used according to the dimensions in Table 6 are placed. Negative and positive pressures were recorded after the explosion. According to the recorded maximum positive pressure, the scaling distance (Z) corresponding to the ambient pressure ( $P_{so}$ ) in the UFC chart in Figure 10 was measured. According to the formulation in Equation 1, the TNT equivalent of the explosive used was determined.

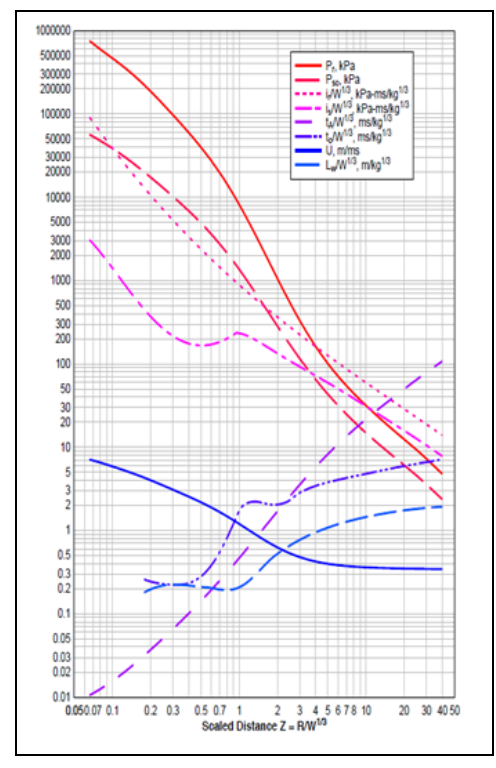


Figure 10. Logarithmic graph of free air blast with scaling factor [44].

Based on the dimensions provided in Table 6, the explosives were positioned, and both negative and positive pressures were measured post-detonation. The recorded maximum positive pressure of  $52.924 \, \text{N/m}^2$  ( $52,924 \, \text{kPa}$ ) yielded a scaled distance (Z) of 3.87, as indicated by the ambient pressure in the UFC chart (Figure 10). Given the explosive-sensor distance of  $3.20 \, \text{m}$ , Equation 1 [44] was utilized to compute the equivalent TNT weight ( $W_{\text{TNT}}$ ) as  $0.57 \, \text{kg}$ . Thus, the TNG explosive is equivalent to approximately 62% of the TNT standard(Equation 2), as indicated in Table 7.

$$\frac{W_{TNG}}{W_{TNT}} = \frac{0.91}{0.57} = 0.62 \tag{2}$$

Table 7. Calculated sensor values

	Max	Pressure	Min	Pressure		
SEN SOR	Time	Pressure (N/m²)	Time	Pressure (N/m²)	Z (m/kg (1/3))	W (kg)
5011	8.590 098	52.924	8.594 297	-11795.8	3.866 359	0.570 274

Figure 11 shows the blast pressure time graph recorded by the DAQ system. The first shock in the graph shows the ambient pressure, and the second shock shows the pressure reflected from the ground. The cumulative impulse-time graph obtained(Fig.12) from the explosion pressure-time curve distinctly illustrates the temporal characteristics of the loading. The graph illustrates that, although the duration of the positive phase is very brief (about 2 ms), it generates a substantial impulse (around 18 kPa·ms). This signifies that the energy imparted to the structure at the moment of the explosion was both intense and abrupt. The negative phase is prolonged (about 20 ms) and has generated an impulse in the contrary direction (approximately –14.5 kPa·ms). Nonetheless, owing to the prevailing influence of the positive phase, the net impulse

value persists as positive (  $3.5 \text{ kPa} \cdot \text{ms}$ ). This instance illustrates that the blast effect is not exclusively contingent upon peak pressure, but is also intricately associated with loading time and the equilibrium between phases. The predominance of the positive phase is crucial in structural deformation and crater formation. Cumulative impulse analysis offers a more dependable metric for comprehending the impact of explosions on structural performance.

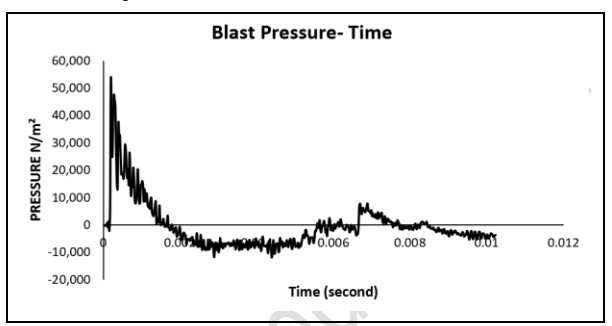


Figure 11. Blast pressure-time graphic.

Total and the second of the se

Figure 12. Cumulative Impuls-time graphic.

#### 4 Placement of samples in the test area

At the blast area of Firat University, the samples were placed at 6 m intervals in order to prevent the interaction of the plates with each other in the explosion as seen in Figure 13.

In order to distribute the explosive charge on the plate uniformly their weights were determined and placed in cube formworks.



Figure 13. Placement of samples on area with explosives.

#### 5 Results and Discussions

The explosive quantity was ascertained based on damage levels. In the explosion region, 133, 266, 399, 532, 665, 798, and 931 g of TNG (equal to 82, 165, 247, 330, 412, 495, and 577 g of TNT) were detonated on unfortified plain sample. The tests

revealed that the concrete slab was fractured on the upper surface with 330 g of TNG, and at the application of 577 g of TNG (equal to 931 g), the structural integrity was entirely compromised, rendering stability unmaintainable. Consequently, in the reinforcement process utilizing geogrid, the selection was predicated on the most adverse circumstance, with 577 g of TNT designated as the threshold value. At reduced quantities, only fissures developed in the samples, although the overall structural integrity was preserved (Fig. 14).



Figure 14. Contact explosion of 266,399,532,665,798 gr TNG explosives, respectively, on unreinforced plates.

When the test results were examined, it was observed that there was no linear correlation between the increase in the number of layers and the crater diameters and depths formed by using 6, 9 and 12 layers of geogrid, respectively. The crater depth of 1.8 cm, which is one of the smallest lengths measured after the experiment, belongs to the 12-layer geogrid (Table 8). The adhesion between the geogrid and the concrete is essential for crack management. Investigations following the explosion indicated that the bond between the geogrid and the concrete inhibited fracture propagation, hence delaying crack formation. Increasing the number of layers from 6 to 12 resulted in the observation of local delamination and interface cracks in regions with inadequate adhesion. This scenario illustrates that geogrid adhesion is essential for material selection and placement specifics. This is due to its ductile characteristic, characterized by a progressive reduction in stress instead of an abrupt release. It absorbed the energy generated by the abrupt explosion load, averting rapid fractures and displacements (Fig. 15).



Figure 15. Post-explosion views of the samples prepared in 6, 9 and 12 layers using geogrid.

Table 8. Crater dimensions of concrete slabs using geogrid material.

Geogrid	Explosive	Crater	Crater	Crater
Samples	Amount	Diameter	Diameter	Depth
. AV	(gr)	X (cm)	Y(cm)	(cm)
Geogrid-6layers	577	12	13	2.2
Geogrid-6layers	577	16	14	2.5
Geogrid-9layers	577	13	12	2.2
Geogrid-9layers	577	13	12	3
Geogrid-12layers	577	11	11	1.8
Geogrid-12layers	577	13	13	3

Plates manufactured using wire mesh; it is a reference sample for geogrid, wire fences and composite concretes. For this purpose, 6 samples were produced for each. In the samples detonated under the effect of 577gr TNT, the maximum crater diameter is 6.7 cm and the maximum crater depth is 2,8 cm. Types of damage observed in samples after explosion According to ACI544[45] and CEB-FIP[46], intense radial cracks and local spalling were observed in samples using wire

mesh after the explosion. However, structural integrity was maintained (Fig. 16).



Figure 16. Crater dimensions of wire steel mesh design.

Samples featuring a mesh size of 4 cm and 5 cm, constructed from galvanized steel wire, were arranged in 7, 10, and 13 layers, respectively, to investigate the shear and punching effects. Wire fences with a 5 cm mesh were cut into 45x45 cm dimensions to be positioned in the formworks and stacked in 7, 10, and 13 layers, then built using concrete with a compressive strength of 35 MPa. Seven layers of wire fence samples with a 5 cm mesh spacing were exploded using 931 grams of explosive. Upon analyzing damage types in wire fence layered samples in accordance with ACI544[45] and CEB-FIP[46], the damage is categorized as mild surface damage. The structural integrity has been maintained through regulated energy transmission. Upon analyzing the crater depth post-explosion in Figures 17 and 18, it is noted that it reached a maximum of 14 cm.



Figure 17. The post-explosion views of the samples prepared in 7, 10 and 13 layers using wire fence.

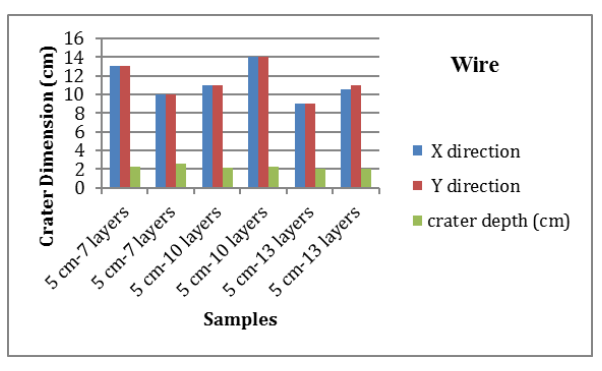


Figure 18. Crater measurements of concrete slabs with 5 cm wire mesh

#### 5.1 Statistical Analysis

The crater diameter and depth data obtained from the experimental studies were first summarized using descriptive statistical methods (Table 9). The mean diameter values between the groups were determined to be in the range of 10.0–13.75 cm, while the depth values were in the range of 2.1–2.6 cm. The low standard deviation values indicate that the experimental results are consistent and that the measurements were reliably repeated. The results of the normal distribution test (Shapiro–Wilk) and the homogeneity of variance test (Levene) showed that the data set did not follow a normal distribution and that the variances were not homogeneous. Therefore, parametric tests (ANOVA) were not considered reliable, and the analyses were continued using the non-

parametric Kruskal-Wallis test. According to the Kruskal-Wallis test results, no statistically significant difference was found between the groups for either crater diameter (p = 0.57) or crater depth (p = 0.44) (Table 10). This finding indicates that the number of geogrid layers or the use of wire mesh has no significant effect on the post-explosion crater geometry. In other words, changes in the type of reinforcement and the number of layers create differences in crack formation and energy absorption mechanisms rather than reducing crater diameter and depth. The Mean ± SD error bar graphs presented in Figure 19 reveal that the average values between groups are quite close to each other. The boxplot graphs show that the median values are in similar ranges and that there are no outliers between groups. These findings support the statistical test results. Therefore, it has been concluded that geogrid and wire mesh reinforcements do not directly change the crater geometry; however, they limit the progression of micro-cracks in particular by affecting the damage mechanism of the material.

Table 9. Descriptive statistics Analysis

-	Tuble 3. 2 everipely e statistics rimary sie								
Sample	Diameter _Mean	Diamet er_SD	Diamet er_Min	Diamete r_Max	Depth_ Mean	Dept h_SD	Depth _Min	Depth _Max	n
Geogrid-12layers	12	1.41	11	13	2.4	0.85	1.8	3	2
Geogrid-6layers	13.75	1.77	12.5	15	2.35	0.21	2.2	2.5	2
Geogrid-9layers	12.5	0	12.5	12.5	2.6	0.57	2.2	3	2
Wire Fence (5 cm diameter) – 10 layers	12.5	2.12	11	14	2.25	0.07	2.2	2.3	2
Wire Fence (5 cm diameter) – 13 layers	10	1.41	9	11	2.1	0	2.1	2.1	2
Wire Fence (5 cm diameter) – 7 layers	11.5	2.12	10	13	2.45	0.21	2.3	2.6	2
Wire Mesh – 4 layers	11.625	1.38	10	13	2.575	0.17	2.4	2.8	4

Table 10. Kruskal-Wallis test results

Chi-Square

Parameter

	Crater Diameter	Kruskal- Wallis	4.79	0.57	
	Crater Depth	Kruskal- Wallis	5.81	0.44	•
3.0 (E.2.) (E.2.	Mean ± SD of Crater Depth		15.0 (W) 12.5 39 10.0 10.0 10.0 10.0 10.0 10.0 10.0 10.0	Crater Diameter by Group	a seed
Office 12 September 12 September 12 September 12 September 13 September 14 Septembe	Boxplot of Crater Diameter is		2-6 0: 2-5 19: 2-7 19: 2-7 2-7 2-7 2-7 2-7 2-7	ater Depth by Group	de

Figure 19. Mean ± SD error bars and boxplot graphs

The slab failure mechanisms identified in experimental research have been categorized according to ACI 544R and the CEB-FIP Model Code 1990. These two standards examine fracture behavior from distinct viewpoints, offering a supplementary foundation for understanding the results acquired. The ACI 544R classification categorizes the fracture

mechanism of fiber-reinforced concrete into three primary groups. Brittle fracture is defined by the abrupt failure of the element due to inadequate fibers following matrix cracking, a phenomenon primarily found in fiber-free and minimally reinforced specimens. Secondly, post-cracking toughness refers to the system's capacity to absorb energy and demonstrate ductility following cracking, attributed to fiber pullout; this failure mode is frequently observed in specimens reinforced with geogrids and wire mesh. The third category, strain-hardening, is defined by the sustained enhancement of load-bearing capacity following matrix cracking, attributed to fiber reinforcement, and has been demonstrated to a limited degree in specimens utilizing multi-layered geogrids. The CEB-FIP Model Code 1990 emphasizes that classification is primarily determined by structural behavior. Punching shear failure manifests as a conical failure surface at the loading point and is prevalent in fiberless or low-layer specimens. Flexural failure is marked by extensive fissures and significant deformations on the underside of the slab, particularly evident in fiberreinforced specimens. Shear failure is characterized by the prevalence of diagonal cracks and has been noted exclusively in the peripheral areas. Furthermore, a combination of failure types has been noted in numerous specimens rather than a singular failure mode. In geogrid-reinforced specimens, the interplay of flexural and punching characteristics has become predominant.The experimental results indicate that the material-centric methodology of ACI 544R enhances the structural behavior-oriented approach of CEB-FIP. Unfibred and minimally reinforced specimens fall under the "sudden failure" classification in ACI 544R and the "punching failure" classification in CEB-FIP. Fiber/geogrid-reinforced specimens align with the "post-crack strength" or "strain-hardening" classification in ACI 544R and the "bending + mixed failure" category in CEB-FIP. The data indicate that the reinforcement features do not directly modify the crater geometry; however, they substantially enhance the energy absorption capacity of the slabs by converting the fracture mode from brittle to ductile behavior.

#### 6 Conclusions

The present study experimentally and statistically examined the behavior of reinforced concrete slabs subjected to contact explosion stress, utilizing several reinforcement materials (geogrid, steel wire mesh, and steel wire fence). The principal conclusions are detailed below:

- The 577 g TNG (931 g TNT equivalent) employed in contact detonations was established as the threshold for structural integrity, taking into account the sample size. Exceeding this threshold resulted in a total loss of slab integrity, whereas lower loads induced cracking while preserving overall structural integrity.
- Geogrid-reinforced plates shown superior efficacy in energy absorption during blasts by restricting crack development. In multi-layer applications, ductile behavior was noted rather than brittle fracture, resulting in a substantial improvement in energy absorption capacity.
- Specimens with steel wire mesh restricted the crater's diameter and depth, hence enhancing structural integrity through more controlled energy dispersion.
- Specimens reinforced with steel wire fence exhibited numerous radial fissures and localized surface detachments, while overall integrity was preserved.

- The Kruskal-Wallis test indicated that neither the kind of reinforcement nor the number of layers produced a statistically significant effect on crater diameter and depth (p > 0.05). This suggests that the damage mechanism pertains to crack formation, energy absorption, and adhesion characteristics rather than crater morphology.
- The ACI 544R categorization indicates that unreinforced specimens demonstrated "sudden failure," but specimens reinforced with geogrid and wire mesh displayed "post-crack resistance/ductile behavior." The CEB-FIP Model Code 1990 categorizes unreinforced plates as experiencing "punching failure," whereas reinforced plates predominantly exhibit "bending and mixed damage" modes. This signifies that the two standards are complementary and that reinforcement elements convert the failure mode from brittle to ductile behavior.

Geogrid and steel wire mesh reinforcements did not directly modify crater geometry; but, by changing the damage type, they restricted crack propagation, enhanced energy absorption capacity, and aided in preserving structural integrity. The findings suggest that geogrid and wire mesh materials may serve as alternatives to steel reinforcement in structures subjected to blast impact, providing a feasible method for enhancing blast resistance. In the analysis of crater diameter and depth, concrete specimens reinforced with geogrid exhibited superior performance. The fissures in these specimens were confined to the micro-crack level and did not inflict damage that would jeopardize structural integrity. This discovery indicates that geogrid reinforcement provides an efficient design method for dissipating blast energy. Moreover, the findings indicate that geogrid material demonstrates comparable performance to steel reinforcement for shear and puncture resistance. Consequently, geogrid material is regarded as a viable substitute for steel reinforcement in constructions subjected to contact explosion.

#### 7 Author contribution statement

Author 1, Literature review, design of the experimental program, implementation and evaluation of the experiments. Author 2, Design of the experiment and control of the experiment.

## 8 Ethics committee approval and conflict of interest statement

"There is no need to obtain permission from the ethics committee for the article prepared".

"There is no conflict of interest with any person / institution in the article prepared".

#### 9 Reference

- [1] Li J, Hao H. "Numerical study of concrete spall damage to blast loads". *International Journal of Impact Engineering*, 68(1), 41–55, 2014.
- [2] Li Q, Wu C, Su Y. "Experiment and numerical investigations of ultra-high toughness cementitious composite slabs under contact explosions". *International Journal of Impact Engineering*, 159(1), 1–20, 2022.
- [3] Brismar BO, Bergenwald L. "The Terrorist Bomb Explosion in Bologna, Italy, 1980". *Journal of Trauma Injury Infection and Critical Care*, 22(3), 216–220, 1982.

- [4] Máca P, Sovják R, Konvalinka P. "Mix design of UHPFRC and its response to projectile impact". *International Journal of Impact Engineering*, 63(1), 158–163, 2014.
- [5] [Li J, Wu C, Hao H, Wang Z, Su Y. "Experimental investigation of ultra-high performance concrete slabs under contact explosions". *International Journal of Impact Engineering*, 93(1), 62–75, 2016.
- [6] Savaş S, Ulker M, Turgut S, Bakir D. "Determination of energy damping upon impact load in reinforced concrete sandwich plates with different core geometries". *Scientia Iranica*, 28(6A), 3082–3091, 2021.
- [7] Wan W, Yang J, Xu G, Liu Y. "Determination and evaluation of Holmquist-Johnson-Cook constitutive model parameters for ultra-high-performance concrete with steel fibers". *International Journal of Impact Engineering*, 156(1), 1–15, 2021.
- [8] Yang D, Zhang B, Liu G. "Experimental Study on Spall Resistance of Steel-Fiber Reinforced Concrete Slab Subjected to Explosion". International Journal of Concrete Structures and Materials, 15(1), 2021.
- [9] Yao W, Sun W, Shi Z, Chen B, Chen L, Feng J. "Blast-resistant performance of hybrid fiber-reinforced concrete (HFRC) panels subjected to contact detonation". *Applied Sciences*, 10(1), 2020.
- [10] Shi S, Liao Y, Peng X, Liang C, Sun J. "Behavior of polyureawoven glass fiber mesh composite reinforced RC slabs under contact explosion". *International Journal of Impact Engineering*, 132(1), 2019.
- [11] Wang W, Yang J, Wang J, Wang X, Huo Q. "Experimental investigation of polyisocyanate-oxazodone coated square reinforced concrete slab under contact explosions". *International Journal of Impact Engineering*, 149(1), 2021.
- [12] Zhao C, He K, Lu X, Pan R, Wang J, Li X. "Analysis on the blast resistance of steel concrete composite slab". *Explosion and Shock Waves*, 41(9), 2021.
- [13] Wang ZG, Wu H, Fang Q, Wu J. "Numerical study on the residual axial capacity of ultra high performance cementitious composite filled steel tube (UHPCC-FST) column under contact explosion". *Thin-Walled Structures*, 153(1), 2020.
- [14] Lakshmi Priyanka C, Vijayalakshmi B, Nagavalli M, Dhinakaran G. "Strength and durability studies on high volume ready-made ultrafine slag-based high-strength concrete". *Scientia Iranica*, 26(5A), 2624–2632, 2019.
- [15] Al-Hedad ASA, Farhan NA, Zhang M, Sheikh MN, Hadi MNS. "Effect of geogrid reinforcement on the drying shrinkage and thermal expansion of geopolymer concrete". Structural Concrete, 21(3), 1029–1039, 2020.
- [16] Dong YL, Han J, Bai XH. "Numerical analysis of tensile behavior of geogrids with rectangular and triangular apertures". Geotextiles and Geomembranes, 29(2), 83–91, 2011.
- [17] Cicek E, Guler E, Yetimoglu T. "Effects of the first reinforcement depth on different types of geosynthetics". *Scientia Iranica*, 26(1A), 167–177, 2019.
- [18] Yadu L, Tripathi RK. "Effect of the Length of Geogrid Layers in the Bearing Capacity Ratio of Geogrid Reinforced Granular Fill-soft Subgrade Soil System". *Procedia Social and Behavioral Sciences*, 104, 225–234, 2013.
- [19] Derakhshandi M, Rahmati G, Sadjadi M. "Static Performance of Geosynthetic Reinforced Soil Walls with Peripheral Soil–Cement Mixtures". *Scientia Iranica*, 0(0), 0–0, 2018.
- [20] Savas S, Bakir D, Akcaat YK. "Experimental and numerical investigation of the usability of nonwoven hemp as a

- reinforcement material". Case Studies in Construction Materials, 20, e03091, 2024.
- [21] Siva Chidambaram R, Agarwal P. "The confining effect of geo-grid on the mechanical properties of concrete specimens with steel fiber under compression and flexure". *Construction and Building Materials*, 71, 628–637, 2014.
- [22] RajeshKumar K et al. "Structural Performance of Biaxial Geogrid Reinforced Concrete Slab". *International Journal* of Civil Engineering, 20, 349–359, 2022.
- [23] Al Qadi ANS, Al-Kadi QNS, Al-Zaidyeen SM. "Impact Strength of Oil-Palm Shell on Lightweight Concrete Slabs Reinforced with a Geo-Grid". *Journal of Materials in Civil Engineering*, 27(10), 04014264, 2015.
- [24] Meng X, Jiang Q, Liu R. "Flexural performance and toughness characteristics of geogrid-reinforced pervious concrete with different aggregate sizes". *Materials*, 14(9), 2021.
- [25] Vijay TJ, Rajesh Kumar K, Vandhiyan R, Mahender K, Tharani K. "Performance of Geogrid Reinforced Concrete Slabs under Drop Weight Impact Loading". *IOP Conference Series: Materials Science and Engineering*, 981(3), 032070, 2020.
- [26] Wu J. "Development of advanced pavement materials system for blast load". National University of Singapore, 2012
- [27] Wu J, Chew SH. "Field performance and numerical modeling of multi-layer pavement system subject to blast load". Construction and Building Materials, 52, 177–188, 2014.
- [28] Chen GF. "Experimental study on axial compression behavior of steel wire confined concrete". *Zhengzhou University*, 2010.
- [29] Emara M, Rizk MS, Mohamed HA, Zaghlal M. "Enhancement of circular RC columns using steel mesh as internal or external confinement under the influence of axial compression loading". *Frattura ed Integrità Strutturale*, 15(58), 86–104, 2021.
- [30] Fahmy EH, Shaheen YBI, Abdelnaby AM, Abou Zeid MN. "Applying the Ferrocement Concept in Construction of Concrete Beams Incorporating Reinforced Mortar Permanent Forms". International Journal of Concrete Structures and Materials, 8(1), 83–97, 2014.
- [31] Kondraivendhan B, Pradhan B. "Effect of ferrocement confinement on behavior of concrete". *Construction and Building Materials*, 23(3), 1218–1222, 2009.

- [32] Tawab AA, Fahmy EH, Shaheen YB. "Use of permanent ferrocement forms for concrete beam construction". *Materials and Structures*, 45(9), 1319–1329, 2012.
- [33] Ibrahim HM. "Experimental investigation of ultimate capacity of wired mesh-reinforced cementitious slabs". *Construction and Building Materials*, 25(1), 251–259, 2011.
- [34] Li J, Wu C, Hao H. "Spallation of reinforced concrete slabs under contact explosion". *Asian Conference on Defence Technology*, 2nd ed., 42–45, 2016.
- [35] Li J, Wu C, Hao H, Su Y. "Experimental and numerical study on steel wire mesh reinforced concrete slab under contact explosion". *Materials and Design*, 116(1), 77–91, 2017.
- [36] DIN EN 10137-3. "Plates and Wide Flats Made of High Yield Strength Structural Steels in the Quenched and Tempered or Precipitation Hardened Conditions Part 3: Delivery Conditions for Precipitation Hardened Steels". Berlin, Germany, 1995.
- [37] ISO 1183-1, "Plastics Methods for determining the density of non-cellular plastics Part 1: Immersion method, liquid pycnometer method and titration method".2025.
- [38] ASTM D1603-20, "Standard Test Method for Carbon Black Content in Olefin Plastics". 2020.
- [39] ISO 9863-1, "Geosynthetics Determination of thickness at specified pressures".2016.
- [40] ISO 9864, "Geosynthetics Test method for the determination of mass per unit area of geotextiles and geotextile-related products".2005.
- [41] "Orica-Nitro Explosives." [Online]. Available: http://www.orica-nitro.com.tr/
- [42] "Oros-Or36-Datalogger." [Online]. Available: https://www.oros.com/solutions/instruments-accessories/or36-mobipack-16-channels-teamwork-analyzer-recorder/
- [43] Savas S, Bakir D. "An experimental study on the blast responses of hollow core concrete slabs to contact explosions," *Rev. la construcción*, 21(3), 587–601, 2022.
- [44] U. F. Criteria(UFC), Structures to Resist the Effects of the Accidental Explosions. 2008.
- [45] ACI 544, State-of-the-Art Report on Fiber Reinforced Concrete, 2002.
- [46] CEB-FIP, Model Code for Concrete Structures, 1990.